Calorimetric Study of Phase Transitions Involving Twist-Grain-Boundary TGB A and TGB C Phases

L. Navailles, C. Garland, H. Nguyen

Calorimetric Study of Phase Transitions Involving Twist-Grain-Boundary TGB_A and TGB_C Phases

L. Navailles ([1,*]), C.W. Garland ([1,**]) and H.T. Nguyen ([2])

([1]) School of Science and Center for Material Science and Engineering, Massachusetts Institute of Technology, Cambridge, Massachusetts 02139, USA
([2]) Centre de Recherche Paul Pascal, avenue A. Schweitzer, 33600 Pessac, France

(Received 16 April 1996, accepted 30 May 1996)

PACS.64.70.Md – Transitions in liquid crystals
PACS.61.30.-v – Liquid crystals
PACS.65.20.+w – Heat capacities of liquids

Abstract. — High-resolution calorimetry has been used to determine the heat capacity and latent heat associated with phase transitions in the homologous series of chiral liquid crystals nF$_2$BTFO$_1$M$_7$ [3-fluoro-4(1-methylheptyloxy)4′-(4″-alkoxy-2″,3″-difluorobenzoyloxy)tolane]. These compounds exhibit smectic-C* (SmC*), twist-grain-boundary (TGB_A for $n = 10$, TGB_C for $n = 11$, 12) and cholesteric (N*) phases. All the phase transitions are first order with small to moderate latent heats. There is a large rounded excess heat capacity peak in the N* phase that is consistent with the predicted appearance of short-range TGB order (chiral line liquid character). This is analogous to the development of an Abrikosov flux vortex liquid in type-II superconductors. Both the $n = 11$ and 12 homologs exhibit two closely spaced transitions in the region where a single $TGB_C - N^*$ transition was expected. This suggests the existence of two thermodynamically distinct TGB_C phases.

Résumé. — Des expériences de calorimétrie haute résolution ont été réalisées pour déterminer les chaleurs spécifiques et les chaleurs latentes associées aux transitions de phase des homologues de la série crystal liquide nF$_2$BTFO$_1$M$_7$: 3-fluoro-4-[-1-méthyl-heptyloxy]-4′-(4″-alcoxy-2″,3″-difluorobenzoyloxy) tolanes. Ces produits présentent la phase smectique C* (SmC*), les phases à torsion par joint de grain (TGB_A pour $n = 10$ et TGB_C pour $n = 11, 12$) et la phase cholestérique (N*). Toutes les transitions de phase sont du premier ordre. La chaleur latente associée à ces transitions est faible ou modérée. Nous observons, dans la phase N*, un grand pic arrondi qui est en accord avec les prédictions de l'apparition d'un ordre TGB à courte distance (liquide de ligne de dislocation). Ce phénomène est l'analogue du liquide de vortex dans les supraconducteurs de type II. Les composés $n = 11$ et 12 présentent, dans la région où nous attendions une transition $TGB_C - N^*$ unique, deux transitions sur un très faible domaine de température. Ce résultat suggère l'existence de deux phases TGB_C thermodynamiquement distinctes.

([*]) *Present address*: G.D.P.C., Université Montpellier II, c.c. 26, Place E. Bataillon, 34095 Montpellier Cedex 05, France
([**]) Author for correspondence (e-mail: cgarland@mit.edu)

1. Introduction

The existence of a twist-grain-boundary (TGB) phase in chiral liquid crystals was predicted theoretically by Renn and Lubensky [1] in 1988 and first demonstrated experimentally in 1989 by Goodby *et al.* [2]. The TGB_A phase combines a helical twist and smectic-A (SmA) layering. This structure consists of a regular stack of periodic grain boundaries separating regions of SmA order, with the layer normal rotated by $\Delta\theta$ across each boundary. The grain boundaries themselves are formed by a grid of parallel screw dislocations. Many of the experimental studies characterizing the structure and properties of a TGB_A phase have been carried out on compounds of the homologous series nP1M7 (methylheptyl-alkoxyphenylpropioloyl-oxybiphenyl carboxylate), which exhibit the phase sequence SmC*-TGB_A-isotropic (I) [2–5].

Recently, there has been a detailed calorimetric study of the phase transitions in the homologous series nFBTFO$_1$M$_7$ [6] with the general formula

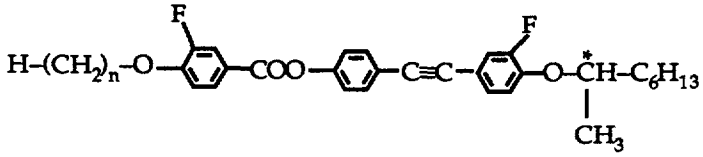

These compounds, whose chemical name is 3-fluoro-4[(R) or (S)-1-methylheptyloxy]4′-(4″-alkoxy-3″-fluorobenzoyloxy) tolan, were synthesized and first characterized by Bouchta *et al.* [7]. For $n \leq 11$, the nFBTFO$_1$M$_7$ compounds exhibit the phase sequence SmA-TGB_A-N*-BP_s-I, where N* is the cholesteric (twisted nematic) phase and BP_s denotes several blue phases. There is an isomorphism between these chiral liquid crystals and high-T_c type-II superconductors in which SmA $\leftrightarrow$ Meissner phase, $TGB_A \leftrightarrow$ Abrikosov flux vortex lattice, N* $\leftrightarrow$ normal metal in a field [1]. Indeed, significant *short-range* TGB structure in the cholesteric phase, corresponding to a *liquid* of screw dislocations (called a chiral line liquid and denoted here as N_L^*), has been predicted by Kamien and Lubensky [8] and is strongly supported by the calorimetric results on nFBTFO$_1$M$_7$ [6]. N_L^* and N* are not thermodynamically distinct phases, but they differ appreciably in the extent of short-range smectic layer formation. The N_L^* region corresponds to the Abrikosov vortex liquid in high-T_c superconductors.

A chiral extension of the liquid crystal model for the N-SmA-SmC multicritical region has led to the theoretical prediction of tilted twist-grain-boundary (TGB_C) phases [9]. Experiments by the Bordeaux group [10–12] on the homologous series nF$_2$BTFO$_1$M$_7$,

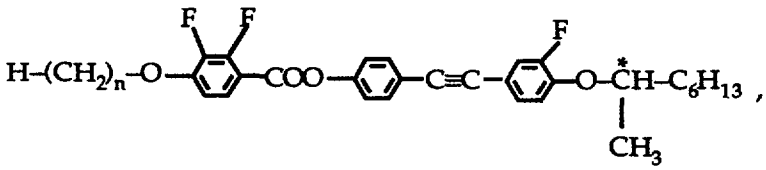

the 2″, 3″-difluorobenzoyloxy analog of nFBTFO$_1$M$_7$, have confirmed the existence of a TGB_C phase. However, the smectic layers in these compounds are tilted relative to the pitch axis [12], in contrast to the structure proposed in reference [9]. In a recent paper, Dozov [13] has proposed the existence of a new phase, called the twist-melted-grain-boundary phase (TMGB). Predicted to be stable close to the N-SmA-SmC* triple point in a chiral liquid crystal, this phase consists of SmC slabs with smectic layers inclined with respect to the pitch axis. It is also argued that the TMGB phase has a lower energy than TGB_C; thus the phase sequence should be SmC*-TMGB-TGB_C-N* (or N_L^*). The major difference between the TMGB and the type of TGB_C

phase reported in reference [12] would be the character of the screw dislocation patterns in the grain boundaries, and this aspect is not yet resolved experimentally.

In the present paper, we report the results of a detailed calorimetric study of $n\mathrm{F_2BTFO_1M_7}$. Three pure compounds ($n = 10$, 11, and 12) and one binary mixture ($n = 10.75$, corresponding to a mixture of 10 and 11 containing 75 mole percent $n = 11$) were investigated with high-resolution ac calorimetry and nonadiabatic scanning calorimetry. The paper is organized as follows. Experimental procedures are briefly summarized in Section 2, and the results are presented in Section 3. A discussion and comparison with results on $n\mathrm{FBTFO_1M_7}$ are given in Section 4.

2. Experimental Methods

A small quantity (typically 50 mg) of each liquid crystal sample was sealed into a thin silver cell containing a helical coil of gold wire to increase the thermal conductivity and eliminate any internal temperature gradients. Details of the sample cell design are given elsewhere [14]. Data were obtained on each sample with a computer-controlled calorimeter capable of both high-resolution ac operation and a nonadiabatic scanning mode [15]. The latter method is a relaxation mode in which the heater power is linearly ramped, and latent heats at first-order transitions can be measured. In both the ac and relaxation mode, the sample temperature is scanned slowly. Heating or cooling rates of 0.02-0.2 K $\mathrm{h^{-1}}$ have been used for ac runs and 2-3.5 K $\mathrm{h^{-1}}$ for relaxation runs. For the ac mode, an oscillating heat input $P_{\mathrm{ac}} \exp(i\omega\tau)$ is supplied to the sample by a thin resistive heater. The frequency ω of the power input is chosen so that $\omega\tau_{\mathrm{int}} \ll 1$, where τ_{int} is the relaxation time for thermal diffusion in the sample cell. The temperature oscillations induced in the sample are slow enough that temperature gradients in the sample are negligibly small and the amplitude T_{ac} of the sample temperature oscillation is given by

$$T_{\mathrm{ac}} = \frac{P_{\mathrm{ac}}}{(R^{-1} + i\omega C)}, \tag{1}$$

where C represents the heat capacity of the sample cell and R is the thermal resistance (reciprocal of the conductance) of the link between the sample and computer controlled thermal bath. In the absence of two-phase coexistence at a first-order transition or complication due to a complex frequency-dependent heat capacity, one finds [15,16]

$$C = \left(\frac{|P_{\mathrm{ac}}|}{\omega|T_{\mathrm{ac}}|}\right)\cos\phi, \tag{2}$$

$$\phi \equiv \Phi + \frac{\pi}{2} = \arctan\left(\frac{1}{\omega RC}\right). \tag{3}$$

where Φ is the phase shift of T_{ac} with respect to P_{ac}. For our calorimeter the standard ac operating frequency is $\omega = 0.196$ (a 32 s period for T_{ac}), for which $\omega\tau_{\mathrm{int}} \ll 1$ and $\omega RC \gg 1$, and ϕ is typically 0.1 to 0.2 rad. The specific heat capacity of the liquid crystal is given by $C_{\mathrm{p}} = [C(\text{filled cell}) - C(\text{empty cell})]/m$, where m is the mass of the liquid crystal.

For the nonadiabatic scanning mode, an effective heat capacity C_{eff} is defined by [15]

$$C_{\mathrm{eff}}(T) = \frac{P - (T - T_{\mathrm{b}})/R}{\mathrm{d}T/\mathrm{d}t}, \tag{4}$$

where P is the dc power input, T is the time-dependent sample temperature, T_{b} is the time-independent bath temperature, and R is the thermal resistance between sample and bath. On

a heating run, $P = 0$ for $t < 0$, $P = \dot{P}t$ for $0 \leq t \leq t_1$, and $P = P_0 = \dot{P}t_1$ for $t > t_1$, where the power ramp rate $\dot{P}$ is constant; on a cooling run, the power profile is reversed. In a one-phase region, C_{eff} is the heat capacity C_p. In a two-phase region, C_{eff} has a large value reflecting latent heat effects associated with conversion of one phase into another. In this case, the latent heat L is given by

$$L = \int_{T_a}^{T_b} [C_{\text{eff}}(T) - C_p(\text{coex})]\text{d}T, \tag{5}$$

where C_p(coex) is the heat capacity of two coexisting phases over the narrow coexistence range from T_a to T_b *in the absence of phase conversion* [6]. The quantity C_p(coex) is obtained by a smooth (typically linear) interpolation between C_p values in the one-phase regions just above and just below the coexistence region. This technique can be used to detect latent heats as small as 0.2 mJ [15].

3. Results

Calorimetric data obtained for $n\text{F}_2\text{BTFO}_1\text{M}_7$ compounds indicate the phase sequences

$$\begin{array}{ll} n = 10 & \text{K} - \text{SmC}^* - \text{TGB}_\text{A} - \text{N}^* - \text{BP}_\text{S} - \text{I} \\ n = 11,\ 12 & \text{K} - \text{SmC}^* - \text{TGB}_\text{C} - \text{N}^* - \text{BP}_\text{S} - \text{I} \end{array}$$

where K denotes a crystalline phase and SmC^* is a chiral tilted smectic phase. At high temperatures, there are typically three blue phases with the sequence $\text{N}^* - \text{BP}_\text{I} - \text{BP}_\text{II} - \text{BP}_\text{III} - \text{I}$, but this region was not studied in detail. It should be noted that the present results support the predicted evolution of the twisted nematic phase from a simple cholesteric (N^*) at high temperatures to a chiral line liquid (N_L^*) with extensive *short-range* TGB order at low temperatures. The possible presence of a narrow range of TGB_A phase in the $n = 11$ homolog, reported in reference [10], will be discussed in Section 4.

An overview of the C_p variation observed with ac calorimetry is given in Figure 1 for the three pure homologs of $n\text{F}_2\text{BTFO}_1\text{M}_7$. The high temperature transitions involving isotropic and blue phases ($T_1 = \text{I} - \text{BP}_\text{III}$, $T_2 = \text{BP}_\text{III} - \text{BP}_\text{II}$, $T_3 = \text{BP}_\text{II} - \text{BP}_\text{I}$, and $T_4 = \text{BP}_\text{I} - \text{N}^*$) will not be discussed here, and attention will be focused on the development of short-range order in the twisted nematic region as well as the transitions involving TGB phases.

3.1. Twisted Nematic Phase. — The excess heat capacity $\Delta C_p = C_p - C_p$(background) associated with the development of N_L^* short-range order in this phase is shown in Figure 2a. These ΔC_p curves are obviously nonsingular since they exhibit neither a divergent peak nor a sharp cusp. However, they can be characterized by their integrated area

$$\delta H = \int \Delta C_p \text{d}T. \tag{6}$$

The possibility of very broad two-phase coexistence due to an extremely sluggish first-order transition can be ruled out by a comparison of C_p(ac) data with C_{eff} values obtained with the nonadiabatic scanning (ramped relaxation) method, as shown in Figure 2b for $n = 10$. If a very broad two-phase coexistence were to occur, there should be a larger excess area observed from nonadiabatic scanning since the latent heat will contribute to C_{eff} but not to C_p(ac). The same sort of match shown in Figure 2b between the broad excess ac heat capacity peak ΔC_p(ac) and that obtained from the nonadiabatic scanning technique was also observed in the $9\text{FBTFO}_1\text{M}_7$ compound investigated in reference [6]. The positions T_5 of this C_p maximum in the twisted nematic phase and the values of the integrated enthalpy δH are given in Table I.

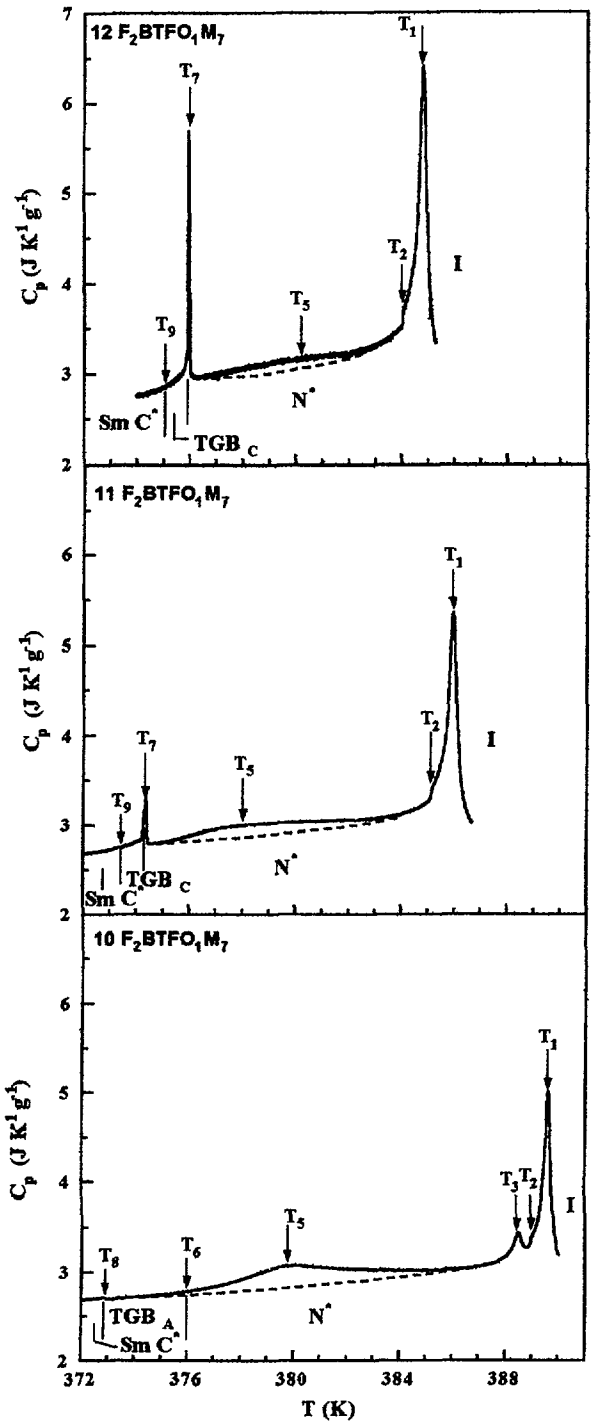

Fig. 1. — Heat capacity of three $n\mathrm{F_2BTFO_1M_7}$ compounds measured with the ac calorimetric mode. The dashed line represents C_p(background), the behavior expected in the N* phase in the absence of short-range TGB ordering.

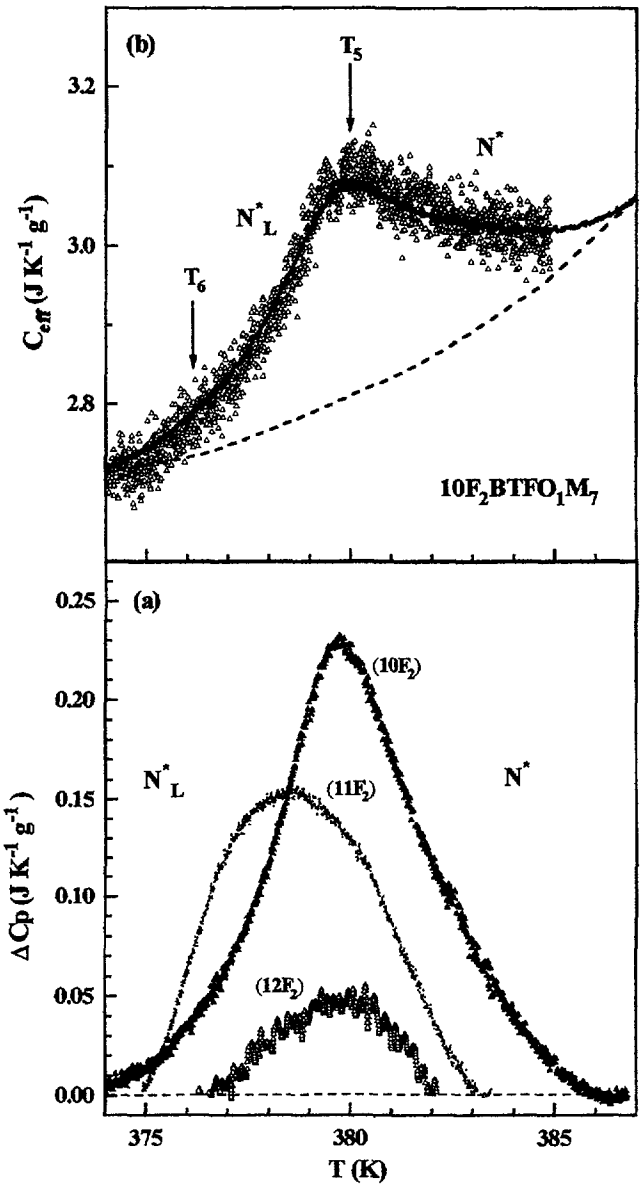

Fig. 2. — (a) Excess heat capacity $\Delta C_p = C_p - C_p$(background) for nF$_2$BTFO$_1$M$_7$ obtained from the ac calorimetric data in Figure 1. N_L^* and N* are *not* distinct phases but represent a cholesteric with and without short-range twisted line liquid structure. (b) $C_{eff}(T)$ data for 10F$_2$BTFO$_1$M$_7$ obtained with the nonadiabatic scanning technique. The smooth curve represents C_p(ac) data from Figure 1, and the dashed curve is C_p(background).

It should be noted that the C_p behavior in the T_5 region was reproducible on both heating and cooling runs obtained over a period of a month. There was, however, a small drift of about -20 mK/day in the position of the ΔC_p maximum. This drift in T_5 is comparable to that observed for the transitions T_6 to T_9 also listed in Table I. The drift rates of these transition temperatures ranged from -7 to -19 mK/day for $n = 10$ and from -14 to -23 mK/day

Table I. — *Transition temperatures (K) and enthalpies (mJ/g) in three $nF_2BTFO_1M_7$ chiral liquid crystals. Higher temperature transitions involving isotropic and blue phases ($T_1 - T_4$) are omitted. In all cases except $N_L^* - N^*$, the transitions are first order with latent heat L and little if any pretransitional excess heat capacity. If the transition temperature is followed by the symbol h, hysteresis was observed (see text for details). T_5 denotes the position of a very broad rounded C_p maximum, but this does not correspond to a phase transition.*

Transition			$n = 10$	$n = 11$	$n = 12$
T_5	$(N_L^* - N^*)$	T_5	380.3 ± 0.5	378.7 ± 0.5	381.2 ± 1.5
		δH	1400 ± 200	700 ± 40	280 ± 50
T_6	$TGB_A - N_L^*$	T_6	376.1 ± 0.2 h		
		L_6	~ 0	–	–
T_{7A}	$TGB_C^\beta - N_L^*$	T_{7A}		375.17 ± 0.02	376.95 ± 0.02
		L_{7A}		~ 125[a]	~ 255[a]
T_{7B}	$TGB_C^\alpha - TGB_C^\beta$	T_{7B}		375.10 ± 0.02	376.90 ± 0.02
		L_{7B}		~ 20[a]	~ 40[a]
		$L_{7A} + L_{7B}$		143 ± 10	297 ± 10
T_8	$SmC^* - TGB_A$	T_8	373.03 ± 0.03 h		
		L_8	70 ± 20		
T_9	$SmC^* - TGB_C^\alpha$	T_9		374.35 ± 0.03 h	376.20 ± 0.05 h
		L_9		52 ± 10	126 ± 10

[a] It is difficult to separate the overall sum $L_{7A} + L_{7B}$ into individual contributions due to the transitions T_{7A} and T_{7B} (see text).

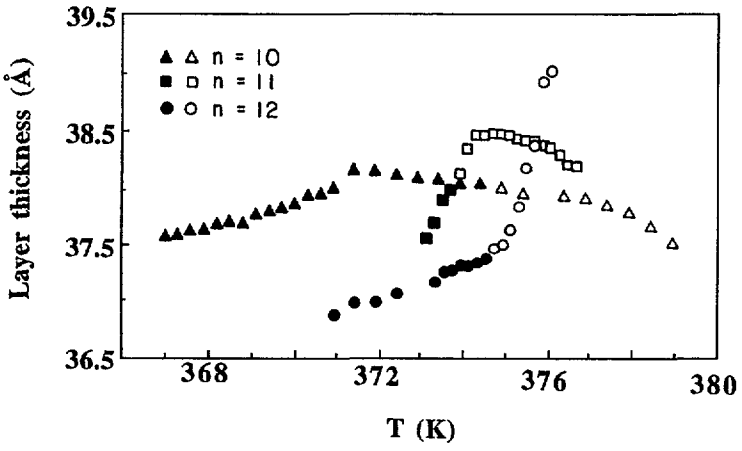

Fig. 3. — Layer spacing d as obtained from an X-ray study of $nF_2BTFO_1M_7$ [10]. The open symbols were obtained from diffuse diffraction peaks, indicating only short-range order, and the solid symbols were obtained from sharp resolution-limited (6.2×10^{-4} Å^{-1}) peaks.

for $n = 11$ and 12. In every case, the temperatures listed in Table I are the values extrapolated back to $t = 0$, based on numerous observations of the transition temperature over times t ranging up to 30 days.

The concept of short-range TGB order evolving in the low-temperature N_L^* region of the twisted nematic phase is supported by X-ray scattering results on $n\mathrm{F_2BTFO_1M_7}$ compounds [10]. Figure 3 displays the "smectic" layer spacing d as a function of temperature for $n = 10$, 11 and 12. Diffuse scattering peaks corresponding to short-range TGB order were observed over a range of several degrees above the transition into the TGB phase. Indeed, in the case of $n = 11$ and 12 there is clear evidence that this short-range order involves tilted smectic character just above the transition temperature, which is reasonable in view of the fact that both these compounds exhibit $\mathrm{TGB_C}$ phases. In contrast, the diffuse scattering in $10\mathrm{F_2BTFO_1M_7}$ is $\mathrm{TGB_A}$ like. It should be noted that due to different samples, different thermometers, and different experimental conditions (length of runs, *etc.*) for the X-ray runs, the transition temperatures inferred from Figure 3 lie 1-2 K lower than those reported in Table I.

The results in Figures 2 and 3 provide strong support for the Kamien-Lubensky [8] theoretical proposal of a chiral line liquid N_L^* in the low-temperature region of the twisted nematic phase. The sequence SmA-$\mathrm{TGB_A}$-N_L^*/N^* is directly analogous to the Meissner-vortex lattice-vortex liquid/normal metal phase sequence in type-II superconductors with thermal fluctuations and weak quenched disorder [17,18]. There is no thermodynamic transition between N_L^*, a twisted nematic with entangled liquid-like (melted) screw dislocation lines, and N^*, a typical cholesteric without short-range TGB order, since these are predicted to have the same macroscopic symmetry [8]. The same argument applies to the Abrikosov vortex liquid and the normal metal in type-II superconductors, and large effects associated with short-range ordering are predicted in that case [17].

3.2. $\mathrm{TGB_A}$-N_L^* TRANSITION. — The $\mathrm{TGB_A}$-N_L^* transition, denoted as T_6 in Table I, is very difficult to detect thermally in either $n\mathrm{FBTFO_1M_7}$ [6,19] or $n\mathrm{F_2BTFO_1M_7}$. Heat capacity C_p and phase shift ϕ data for $10\mathrm{F_2BTFO_1M_7}$ obtained with the ac mode using a slow scan rate (50 mK/h) are shown in Figure 4. Both heating and cooling runs were made. In both cases, the phase ϕ shows a small anomalous maximum that is consistent with two-phase coexistence at a first-order transition; see Figure 2 in reference [6] for the comparable feature in $10\mathrm{FBTFO_1M_7}$ and references [14–16] for a more general discussion. The position of the maximum in ϕ on heating agrees exactly with that of the tiny anomalous "spike" in C_p (heat) shown in Figure 4, whereas the ϕ(cool) maximum lies at a slightly lower temperature. Thus there is a small hysteresis of 0.07 K. Unfortunately, the latent heat at T_6 is too small to be detected with our nonadiabatic scanning technique; thus L_6 is estimated to be less than 3 mJ/g. In the very similar system $n\mathrm{FBTFO_1M_7}$, the latent heat for $\mathrm{TGB_A}$-N_L^* in the $n = 9$ homolog is 8.1 ± 1.2 mJ/g [6] and there are qualitative indications that this latent heat is smaller for $n = 10$ and 11 [19].

3.3. $\mathrm{SmC^*} - \mathrm{TGB_A}$ TRANSITION. — The heat capacity variations on heating and cooling through the $\mathrm{SmC^*} - \mathrm{TGB_A}$ transition, denoted as T_8 in Table I, are shown in Figure 5. The absolute C_p values for these runs are somewhat lower than those observed in earlier runs, and the reasons for this are unclear. In any event the transition features are obvious. A hysteresis of 0.16 K was observed; and phase shift anomalies (not shown), as well as the C_p data, indicate a two-phase coexistence range of ~ 0.30 K on both heating and cooling. These ac mode indications of a first-order transition are confirmed by a latent heat $L_8 = 70 \pm 20$ mJ/g measured with the nonadiabatic scanning mode. The C_p ($\mathrm{SmC^*} - \mathrm{TGB_A}$) behavior shown in Figure 5 is qualitatively the same as that observed in $11\mathrm{FBTFO_1M_7}$ [19].

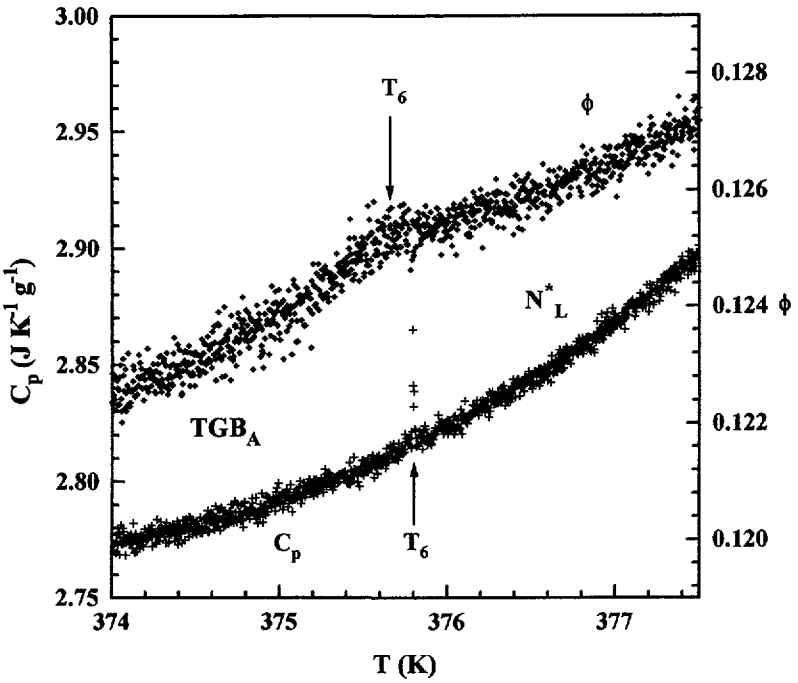

Fig. 4. — Heat capacity C_p and phase shift ϕ near T_6, the $TGB_A - N_L^*$ transition temperature, for $10F_2BTFO_1M_7$. These ac mode C_p data were obtained on heating at a scan rate of 50 mK/h, and the ϕ data are from a cooling scan at −50 mK/h.

3.4. TGB_C-N_L^* TRANSITIONS. — The C_p and phase shift ϕ variations obtained by ac calorimetry in the vicinity of the transition from N_L^* to TGB_C are shown for the $n = 11$ and 12 homologs in Figures 6 and 7. For both compounds, multiple runs were carried out at low scan rates (15-50 mK/h) on heating and on cooling. Although earlier results [10] indicated a single TGB_C-N^* transition, Figures 6 and 7 show two major features denoted as T_{7A} and T_{7B}. In the case of $11F_2BTFO_1M_7$, there is even a very tiny third peak in C_p located 0.09 K above the T_{7A} peak. This small feature was reproducible on seven scans made over a period of 30 days. No hysteresis was observed for any of these C_p peaks although there were slow drifts of −23 mK/day for T_{7A} and T_{7B} and −14 mK/day for the small peak 90 mK above T_{7A}.

The ac calorimetry data in Figures 6 and 7 correspond to what one would expect from two closely spaced first-order transitions. It is known from X-ray studies [10–12] that the phase between the N_L^* region and the SmC^* domain is a tilted TGB structure. Thus we have designated two TGB_C phases - TGB_C^α over the ~ 0.7 K range between T_9 and T_{7B} and TGB_C^β over the narrow ~ 0.06 K range from T_{7B} to T_{7A}. TGB_C^α should correspond to the TGB_C structure experimentally established in reference [12], whereas the structure of the TGB_C^β phase is unknown.

In an effort to determine the latent heats L_{7A} and L_{7B} associated with this pair of closely spaced transitions, nonadiabatic scanning runs were carried out on both the $n = 11$ and 12 homologs and the results are given in Figures 8 and 9. Due to the relatively fast scan rates required for nonadiabatic scanning, it was not possible to resolve two transition features in the N_L^* to TGB_C (T_7) region. So we could determine only the sum of latent heats $L_{7A} + L_{7B}$, which was 143 ± 10 mJ/g for $11F_2BTFO_1M_7$ and 297 ± 10 mJ/g for $12F_2BTFO_1M_7$. As a very

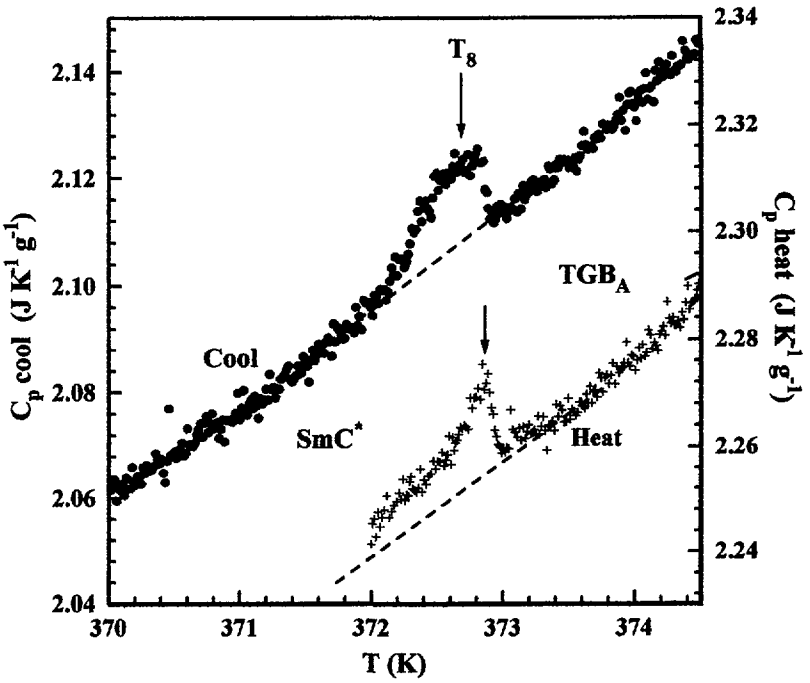

Fig. 5. — Heat capacity measured with the ac mode near T_8, the SmC* – TGB_A transition temperature, for $10F_2BTFO_1M_7$. Scan rates were ±200 mK/h.

rough approximation, we have assumed that the relative size of L_{7A} and L_{7B} can be estimated from the relative size of the integrated excess C_p(ac) peaks. For both $n = 11$ and 12, the ratio C_p (7A) area/C_p(7B) area is about 6.5 and this yields the estimated L_{7A} and L_{7B} values given in Table I.

3.5. SmC* – TGB_C TRANSITION. — The ac heat capacity and phase shift ϕ associated with the SmC* – TGB_C^{α} (T_9) transition in the $n = 11$ and 12 homologs are given in Figures 10 and 11. Both C_p and ϕ show only steps rather than peaks like those observed at T_7 and T_8. However, there are two compelling indications of first-order character: the large C_{eff} peaks at T_9 shown in Figures 8 and 9 for nonadiabatic scanning runs and yielding latent heats $L_9 = 52 \pm 10$ mJ/g for the $n = 11$ compound and $L_9 = 126 \pm 10$ mJ/g for the $n = 12$ homolog; a substantial hysteresis for ac heating and cooling runs (0.85 K for $n = 11$ and 0.50 K for $n = 12$). Furthermore, this thermal behavior is exactly the same as that observed at the analogous SmA – TGB_A transition in nFBTFO$_1$M$_7$ compounds, where the latent heat is reported to be 40 ± 1.6 mJ/g for 9FBTFO$_1$M$_7$ [6]. The relatively large error bounds for the present L_9 and $(L_{7A} + L_{7B})$ values reflects the uncertainty on how to apportion the excess C_{eff} that lies in the temperature range between T_7 and T_9 in Figures 8 and 9.

3.6. MIXTURE. — Nonadiabatic scanning and ac calorimetric runs were also carried out on $10.75F_2BTFO_1M_7$, a binary mixture containing 75 mole percent of the $n = 11$ compound. A broad C_p maximum observed in the N* phase was completely consistent with those seen for the $n = 10$ and $n = 11$ compounds. This T_5 peak was located at 377.9 K and had an integrated area δH of 1200 ± 200 mJ/g. At lower temperatures, a complicated C_p behavior was observed

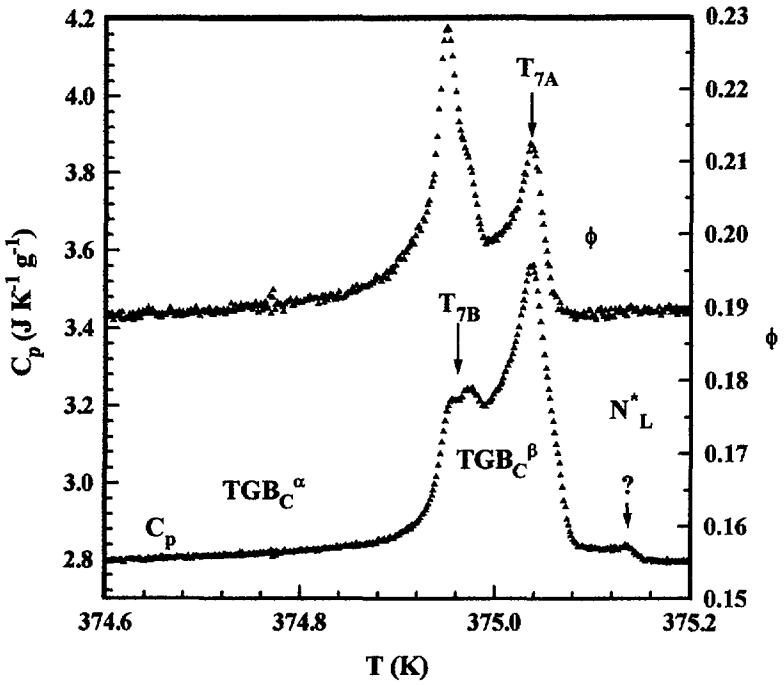

Fig. 6. — Heat capacity and phase shift ϕ for $11F_2BTFO_1M_7$ in the N_L^* to TGB_C transition region. These ac calorimetric data were obtained on heating at a scan rate of 22 mK/h.

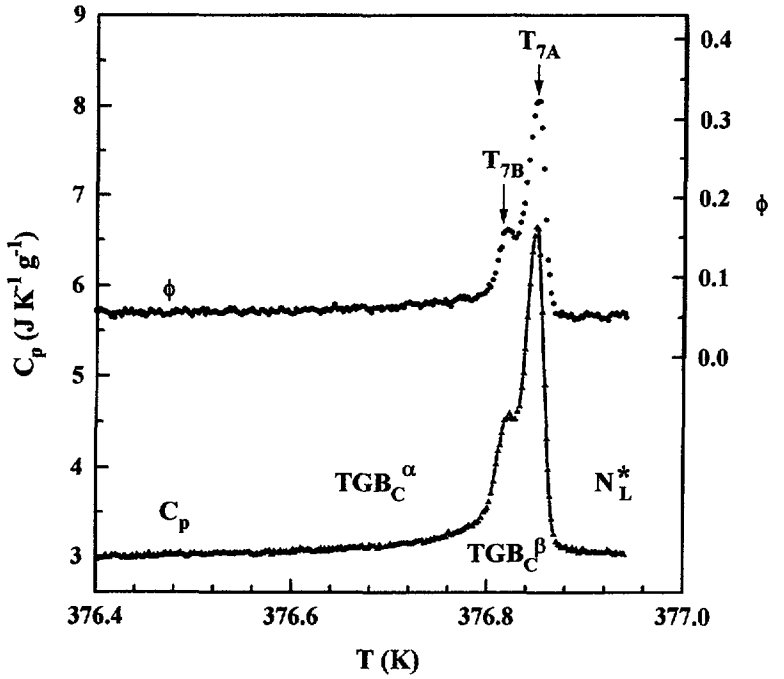

Fig. 7. — Heat capacity and phase shift ϕ for $12F_2BTFO_1M_7$ in the N_L^* to TGB_C transition region. These ac calorimetric data were obtained on cooling at a scan rate of −30 mK/h.

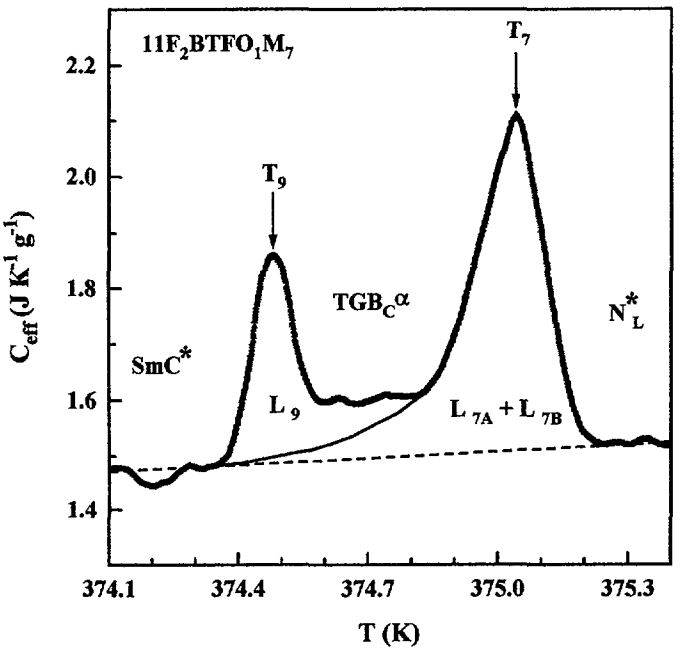

Fig. 8. — $C_{\text{eff}}(T)$ data for $11F_2BTFO_1M_7$ obtained with the nonadiabatic scanning technique at a scan rate of +3.5 K/h. The dashed line represents C_p(coex); see the text. The area under the peak labelled T_7 is 143 mJ/g and corresponds to the sum of latent heats $L_{7A} + L_{7B}$, and the area of 52 mJ/g under peak T_9 represents the latent heat L_9.

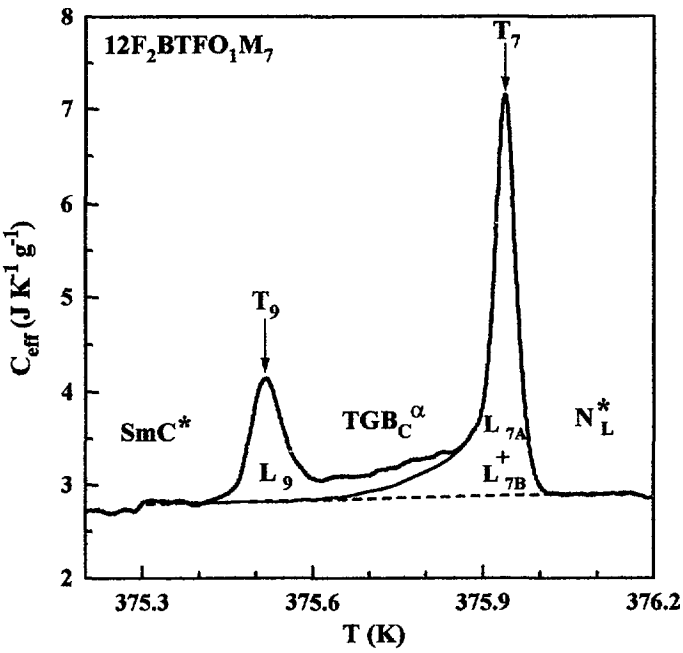

Fig. 9. — $C_{\text{eff}}(T)$ data for $12F_2BTFO_1M_7$ obtained with the nonadiabatic scanning technique at a scan rate of +3.5 K/h. The T_7 area is 297 mJ/g and corresponds to the sum of latent heats $L_{7A} + L_{7B}$, and the T_9 area representing L_9 is 126 mJ/g.

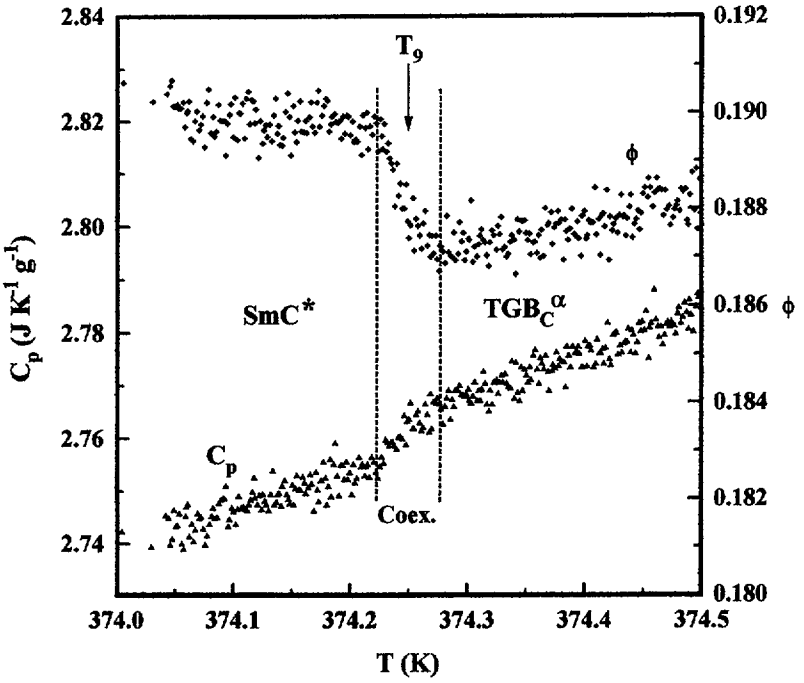

Fig. 10. — Heat capacity and phase shift ϕ for $11F_2BTFO_1M_7$ in the SmC* to TGB_C transition region. These ac calorimetric data were obtained on heating at a scan rate of 22 mK/h.

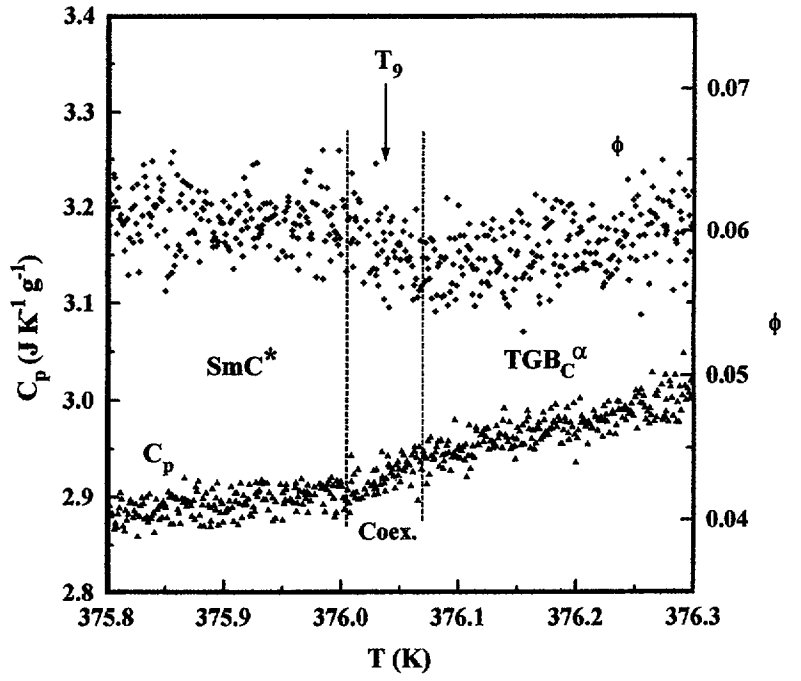

Fig. 11. — Heat capacity and phase shift ϕ for $12F_2BTFO_1M_7$ in the SmC* to TGB_C transition region. These ac calorimetric data were obtained on heating at a scan rate of 15 mK/h.

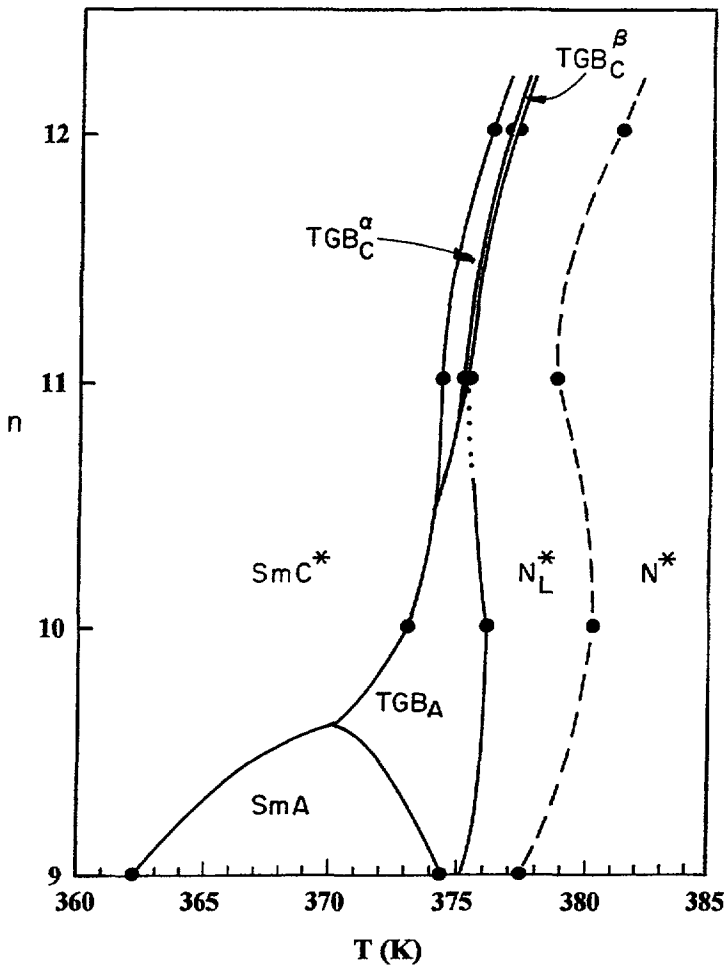

Fig. 12. — Proposed phase diagram for $n\mathrm{F_2BTFO_1M_7}$ based on transition temperatures for $n = 10$, 11 and 12 determined in the present work and corrected DSC data [12] for $n = 9$. The dashed line does not indicate a transition but merely the locus of a C_p maximum in the twisted nematic range.

over the range 372.4 – 373.4 K. For a nonadiabatic scanning run on heating, four peaks were observed at ~ 373.3 K, ~ 373.1 K, ~ 372.8 K, and ~ 372.6 K. The total latent heat associated with these four features was ~ 70 mJ/g. However, only the 373.1 K and 373.3 K peaks were reproducible on nonadiabatic cooling runs and with ac calorimetry. The interpretation of these low temperature $n = 10.75$ features is unclear, and more detailed work with mixtures would be helpful.

4. Discussion

A tentative phase diagram based on data for the $n = 10$, 11, and 12 compounds from the present study combined with DSC data obtained in Bordeaux [10] for $n = 9$ and binary mixtures of $10 + 11$ and $11 + 12$ is given in Figure 12. Comparison of $n\mathrm{F_2BTFO_1M_7}$ transition temperatures obtained with high-resolution calorimetric techniques with those obtained from

DSC show that the DSC temperatures are systematically low by ~ 0.7 K, which is consistent with the results from the study of nFBTFO$_1$M$_7$ [19]. To avoid confusion, ten closely spaced and somewhat scattered DSC points for the mixtures are not shown, but these mixture data given in reference [10] confirm the width of the TGB_C^{α} region and in particular show that a TGB_C phase persists down to $n \simeq 10.5$. The DSC mixture data are also consistent with the dashed N_L^*/N^* line (T_5). Since no mixtures of $n = 9$ and $n = 10$ have been studied, the position of the SmA – SmC* – TGB_A point as well as the SmA – SmC* and SmA – TGB_A lines is speculative but topologically reasonable in view of theory [9] and data on nFBTFO$_1$M$_7$ [6].

The most important new feature of Figure 12 is the fact that the dashed N_L^*/N^* line does not represent a thermodynamic transition but the evolution of *short-range* TGB order. The large excess heat capacity peak (T_5) in the N* phase that is consistent with the predicted evolution of short-range chiral line liquid (N_L^*) character decreases in magnitude from 1.4 J/g for 10F$_2$BTFO$_1$M$_7$ to 0.28 J/g for 12F$_2$BTFO$_1$M$_7$. The same trend was observed for nFBTFO$_1$M$_7$, but the magnitudes were larger (1.8 J/g for 9FBTFO$_1$M$_7$ to 0.82 J/g for 11FBTFO$_1$M$_7$) [6,19].

The extremely small latent heat associated with the TGB_A-N_L^* (T_6) transition in 10F$_2$BTFO$_1$M$_7$ is consistent with the small TGB_A-N_L^* latent heat of 8.1 mJ/g for 9FBTFO$_1$M$_7$ [6] and indicates that the short-range TGB_A order in the N_L^* phase is very well developed just above this transition. In contrast to this, the enthalpy on going from N_L^* to TGB_C^{α} is considerably larger (150-300 mJ/g). It would appear that δH at T_5 is correlated to whether the short-range TGB character in N_L^* is TGB_A-like (large δH) or TGB_C-like (small δH). As noted above, when δH (T_5) is large the latent heat for N_L^* – TGB_A transition is very small in contrast to the moderately large N_L^* – TGB_C latent heats observed when δH (T_5) is small. It seems likely that as the alkoxy chain grows (n increases) the short-range TGB structure in N_L^* develops a TGB_C character, which is supported by the nature of the diffuse scattering shown in Figure 3. Detailed synchrotron structure studies would be of considerable interest.

All the transitions shown in Figure 12 are first order except for SmC* – SmA. Although the latter transition was not observed in the present work, it was found to exhibit typical Landau mean-field second-order behavior in 10FBTFO$_1$M$_7$ and 10.5FBTFO$_1$M$_7$ [19], and the same behavior would be expected in nF$_2$BTFO$_1$M$_7$ samples.

The second important new feature of Figure 12 is the fact that both the $n = 11$ and 12 pure homologs exhibit two closely spaced transitions, indicating that there is a different TGB phase, denoted by TGB_C^{β}, lying between N_L^* and TGB_C^{α}. The structural difference between TGB_C^{α} and TGB_C^{β} is not known. One might speculate that TGB_C^{β} is an incommensurate TGB_C phase or a TGB_C phase with a structure like that originally proposed by Renn and Lubensky [9], and X-ray data [12] on 12F$_2$BTFO$_1$M$_7$ shows that TGB_C^{α} is either a commensurate TGB_C phase or a TMGB phase.

One aspect of the proposed phase diagram that is still unresolved is the detailed behavior of the N_L^* – TGB_A line as it terminates at one of the TGB_C phases. There are many topologically valid possibilities and not yet enough data. Indeed, a narrow range of TGB_A phase was originally reported [10] for $n = 11$ although Figure 3 would suggest that this was due to well-developed short-range TGB_A character in the N_L^* phase just above the N_L^* – TGB_C transition. However, a racemic sample of 11F$_2$BTFO$_1$M$_7$ exhibits the phase sequence N-SmA-SmC [10], which suggests that TGB_A should be stable close to $n = 11$ in the chiral compound. Since the N_L^* – TGB_A latent heat is so small in nF$_2$BTFO$_1$M$_7$, calorimetric measurements are not an ideal way to resolve this issue. Indeed, one might speculate that the tiny C_P feature denoted by the question mark in Figure 6 could correspond to a N_L^* – TGB_A transition. A high-resolution X-ray study that clearly distinguishes diffuse and resolution-limited features is needed to answer such issues.

Acknowledgments

This work was supported primarily by the MRSEC program of the National Science Foundation under Award Number DMR-9400334. We wish to thank P. Barois for helpful discussions and Z. Kutnjak for assistance with several experimental aspects.

References

[1] Renn S.R. and Lubensky T.C., *Phys. Rev. A* **38** (1988) 2132.
[2] Goodby J.W., Waugh M.A., Stein S. M., Chin E., Pindak R. and Patel J., *Nature (London)* **337** (1989) 449; Strajer G., Pindak R., Waugh M.A. and Goodby J.W., *Phys. Rev. Lett.* **64** (1990) 1545.
[3] Huang C.C., Lin D.S., Goodby J.W., Waugh M.A., Stein S.M. and Chin E., *Phys. Rev. A* **40** (1989) 4153.
[4] Ihn K.J., Zasadzinski J.A.N., Pindak R., Slaney A.J. and Goodby J., *Science* **258** (1992) 275.
[5] Goodby J.W., Nishigama I., Slaney A.J., Booth C.J. and Toyne K.J., *Liq. Cryst.* **14** (1993) 37.
[6] Chan T., Garland C.W. and Nguyen H.T., *Phys. Rev. E* **52** (1995) 5000.
[7] Bouchta A., Nguyen H.T., Achard M.F., Hardouin F., Destrade C., Twieg R.J., Maaroufi A. and Isaert N., *Liq. Cryst.* **12** (1992) 575.
[8] Kamien R.D. and Lubensky, T.C., *J. Phys. I France* **3** (1993) 2131.
[9] Renn S.R. and Lubensky T.C., *Mol. Cryst. Liq. Cryst.* **209** (1991) 349.
[10] Nguyen H.T., Bouchta A., Navailles L., Barois P., Isaert N., Twieg R.J., Maaroufi A. and Destrade C., *J. Phys. II France* **2** (1992) 1889; Navailles L., Ph.D. thesis, Univ. Bordeaux I, 1994 (unpublished).
[11] Navailles L., Barois P. and Nguyen H.T., *Phys. Rev. Lett.* **71** (1993) 545.
[12] Navailles L., Pindak R., Barois P. and Nguyen H.T., *Phys. Rev. Lett.* **74** (1995) 5224.
[13] Dozov I., *Phys. Rev. Lett.* **74** (1995) 4245.
[14] Garland C.W., *Thermochim. Acta* **88** (1985) 127.
[15] Yao H., Chan T. and Garland C.W., *Phys. Rev. E* **51** (1995) 4585.
[16] Garland C.W., "Calorimetric Studies" in Liquid Crystals: Physical Properties and Phase Transitions, S. Kumar Ed. (Oxford Univ. Press, in press) Chap. 6.
[17] Fisher D.S., Fisher M.P.A. and Huse D.A., *Phys. Rev. B* **43** (1991) 130 and references cited therein; Huse D.A., Fisher M.P.A. and Fisher D.S., *Nature* **358** (1992) 553.
[18] Nelson D.R., in Phase Transitions and Relaxation in Systems with Competing Energy Scales, NATO Advanced Study Institute, Series B: Physics, T. Riste and D. Sherrington Eds. (Kluwer, 1993).
[19] Chan T., Ph.D. thesis, Massachusetts Institute of Technology (1995) (unpublished).